High Efficiency and Optical Anisotropy in Double-Heterojunction Nanorod Light-Emitting Diodes

Sooji Nam,[†] Nuri Oh,[†] You Zhai, and Moonsub Shim*

Department of Materials Science and Engineering and Frederick Seitz Materials Research Laboratory, University of Illinois at Urbana—Champaign Urbana, Illinois 61801, United States. [†]These authors contributed equally to this work.

ABSTRACT Recent advances in colloidal quantum dot light-emitting diodes (QD-LEDs) have led to efficiencies and brightness that rival the best organic LEDs. Nearly ideal internal quantum efficiency being achieved leaves light outcoupling as the only remaining means to improve external quantum efficiency (EQE) but that might require radically different device design and reoptimization. However, the current state-of-the-art QD-LEDs are based on spherical core/shell QDs, and the effects of shape and optical anisotropy remain essentially unexplored. Here, we demonstrate solution-processed, red-emitting double-heterojunction nanorod (DHNR)-LEDs with efficient hole transport exhibiting low threshold voltage and high brightness (76 000 cd m^{-2}) and efficiencies (EQE = 12%, current efficiency = 27.5 cd A^{-1}, and power efficiency = 34.6 lm W^{-1}). EQE exceeding the expected upper limit of ~8% (based on ~20% light outcoupling and solution photoluminescence quantum yield of ~40%) suggests shape anisotropy and directional band offsets designed into DHNRs play an important role in enhancing light outcoupling.

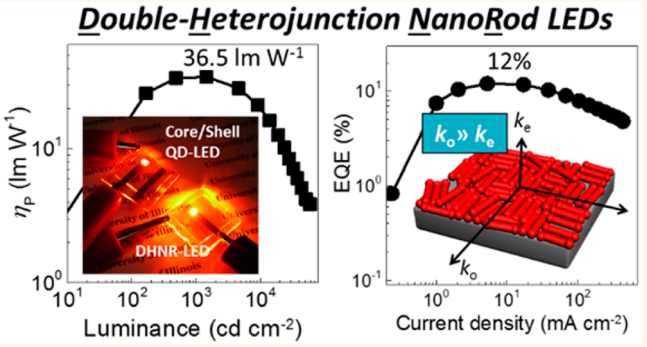

KEYWORDS: double-heterojunction nanorods · light-emitting diodes · high efficiencies · optical anisotropy · light outcoupling

Advances in colloidal quantum dot (QD) light-emitting diodes (LEDs) have led to efficiencies and brightness comparable to and driving voltage lower than those of organic LEDs (OLEDs), reaching an apparent limit on internal quantum efficiency (IQE).[1−4] Building on achievements in OLEDs, device architectures involving an organic hole transport layer (HTL), core/shell (C/S) QD emitters, and an oxide electron transport layer (ETL) have led to the best performing QD-LEDs thus far.[1−4] One of the most promising architectures is the organic hole injection layer (HIL), organic HTL, C/S QDs, and oxide ETL all spin-cast sequentially on indium tin oxide (ITO) with a final Al cathode.[3−7] This device design, which we refer to as the "conventional" device structure, allows convenient and scalable all solution processing (with the exception of the electrodes) and the top inorganic layers may also help to protect organics underneath. However, efficiencies of most of these QD-LEDs have remained modest with maximum external quantum efficiency (EQE) < 2%. One of the main reasons for the less-than-ideal performance is the large offset between HTL Fermi level and the valence band edge of QDs, leading to a large hole injection barrier (HIB).[7] Furthermore, solubility of organic HTLs in solvents for QDs can cause damage or intermixing.[8] Recent introduction of the inverted structure, where ITO is the cathode and Al the anode with vacuum-deposited organic HTL and oxide HIL, has alleviated these problems, rendering efficiencies and brightness of QD-LEDs comparable to those of the best phosphorescent OLEDs while achieving smaller bandwidth and driving voltage.[1,2,9] However, fabrication of QD-LEDs has become more cumbersome, requiring both solution and vacuum deposition. More importantly, nearly ideal IQE being reached[1] leaves no obvious room for improvement other than drastically altering device design for better light outcoupling then reoptimizing to achieve high IQEs. Hence, simple

* Address correspondence to mshim@illinois.edu.

Received for review November 19, 2014 and accepted January 7, 2015.

Published online January 07, 2015
10.1021/nn506577p

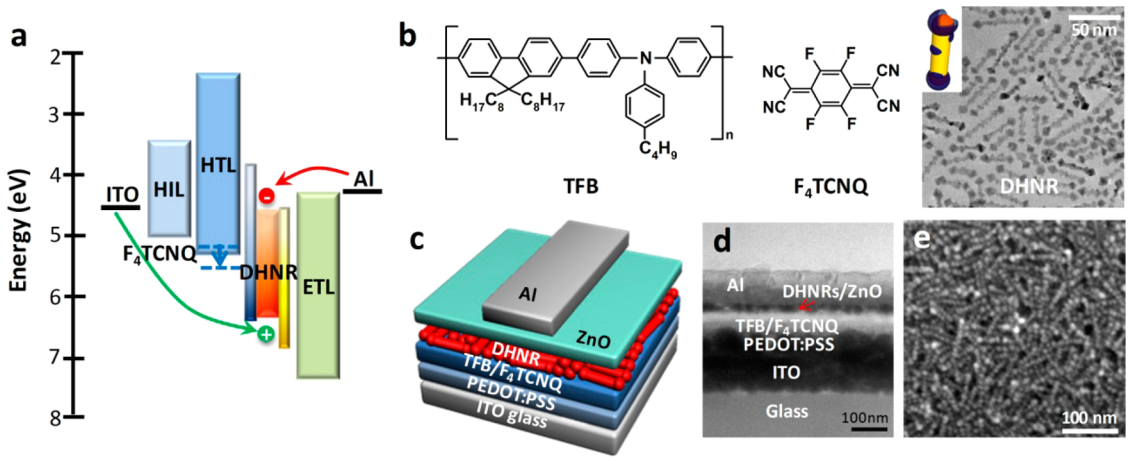

Figure 1. (a) Energy band diagram of DHNR-LEDs. (b) Chemical structure of TFB and F_4TCNQ, and schematic and TEM image of DHNRs. (c and d) Schematic and cross-sectional TEM image of the DHNR LEDs. (e) SEM image of spin-cast DHNRs on TFB/F_4TCNQ HTL.

improvements that simultaneously enable solution deposition and enhanced light extraction are highly desirable.

Heterostructures based on semiconductor nanorods[10−16] are an emerging class of materials that represent a relatively unexplored domain especially with respect to LED applications. Optical anisotropy of nanorod heterostructures may provide additional benefits such as polarized light emission.[17,18] However, non-C/S QD-based LEDs have suffered from poor efficiencies and there have only been a limited number of studies.[17,18] Here, we examine recently developed double-heterojunction nanorods (DHNRs)[19] as the light emitting layer in LEDs with improved hole injection/transport. We demonstrate that DHNR-LEDs surpass C/S QD-LEDs fabricated in the same manner in all performance metrics examined (EQE, current and power efficiencies, and brightness). Consideration of optical anisotropy in improving device characteristics suggests a fundamentally different and higher efficiency limit to these DHNR-LEDs.

RESULTS AND DISCUSSION

The DHNR, where type II staggered band offset semiconductors surround a smaller band gap emitter,[19] represents an especially interesting platform to examine how structural, electronic, and optical anisotropies affect device characteristics. A key enabling feature of DHNRs is that both outer components are physically in contact with the emitting core (CdS and ZnSe outer components and CdSe emitting center for the system examined here), which allows independent control over the electron and hole processes. This feature has allowed a reduction in HIB while maintaining efficient electron injection and a simple replacement of C/S QDs with DHNRs into the conventional QD-LED structure has led to significant improvements.[19] However, HIB due to the high HTL Fermi level and the solvent compatibility issue still remain significant. Once these shortcomings can be addressed, DHNRs may allow shape/optical anisotropy, directional type II band offset, and rod orientation to be exploited in enhancing device performance and enabling new capabilities.

We have introduced 2,3,5,6-tetrafluoro-7,7,8,8-tetracyanoquinodimethane (F_4TCNQ), a well-known p-dopant for conjugated organics and related materials,[20−22] to reduce HIB and improve IQE while maintaining convenient solution processing. Figure 1 shows the band diagram, chemical structures of the key components, device schematic and transmission electron microscopy (TEM) images of DHNRs and DHNR-LEDs. The DHNRs consist of seed CdS nanorod (27.6 nm average length and 4.1 nm average diameter) with CdSe grown at the tips (average diameter of the emitter 4.1 nm) and a ~0.7 nm ZnSe shell mostly around CdSe as shown in the schematic image. Scanning electron microscopy (SEM) of DHNRs spin-cast on poly[(9,9-dioctylfluorenyl-2,7-diyl)-*co*-(4,40-(*N*-(4-*s*-butylphenyl))diphenylamine)] (TFB)/F_4TCNQ HTL indicates that DHNRs are primarily oriented parallel to the device plane (Figure 1e). Naïvely, this orientation and the double-tipped nature of DHNRs may appear unfavorable, *i.e.*, vertically aligned single-tipped counterpart can have ZnSe and CdS selectively contact their corresponding transport layers. However, as discussed later, parallel orientation of DHNRs can have a profound impact on light outcoupling.

Ultraviolet photoelectron spectroscopy (UPS) indicates a monotonic increase in the ionization potential of HTL from 5.35 to 5.54 eV with increasing F_4TCNQ doping (Figure 2a), leading to a lowering of HIB (Figure 2 inset). Key energy levels with different amounts of F_4TCNQ are given in Supporting Information Table S1. The reduction in HIB up to 190 meV is in addition to that provided by the DHNR design (~400 meV by injecting holes through ZnSe rather than CdS). F_4TCNQ also improves HTL conductivity to

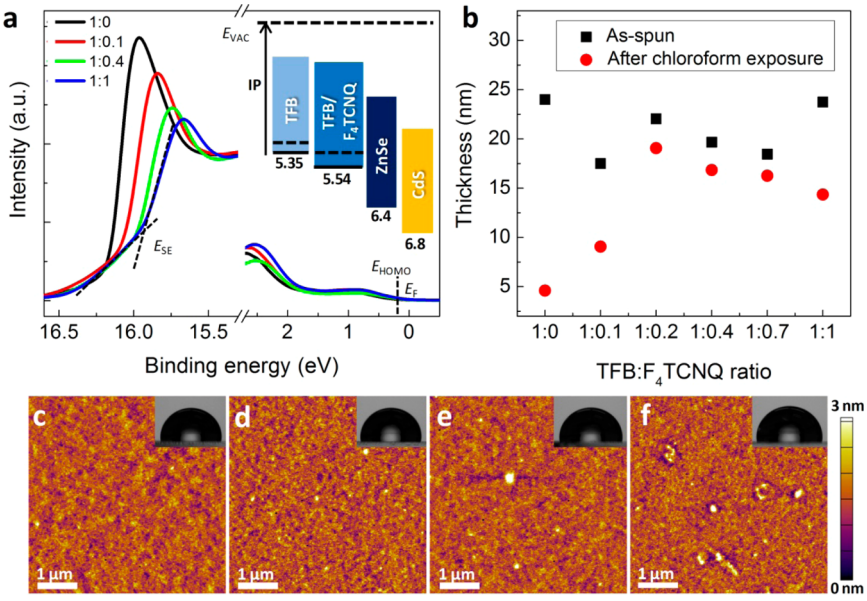

Figure 2. (a) Secondary electron cutoff and the highest occupied molecular orbital (HOMO) regions of the UPS spectra for HTL films with indicated TFB/F_4TCNQ weight ratios. Inset shows the Fermi level positions (dashed lines) and ionization potentials (IP) of TFB and TFB with F_4TCNQ along with valence band edges of ZnSe and CdS of DHNRs. (b) Thickness change of HTL with indicated TFB/F_4TCNQ weight ratios before and after chloroform exposure. (c–f) AFM and water contact angle (insets) images of TFB films with 1:0 (c), 1:0.1 (d), 1:0.4 (e), and 1:1 (f) TFB/F_4TCNQ weight ratio. The root-mean-square surface roughness of the F_4TCNQ doped TFB films with 1:0, 1:0.1, 1:0.4, and 1:1 weight ratios are 0.26, 0.32, 0.38, and 0.42 nm, respectively. The corresponding water contact angles are 101°, 101°, 102°, and 103°, respectively. We note that at 1:1 weight ratio, F_4TCNQ appears to have already reached solubility limit, which may explain the slightly larger change in thickness upon solvent exposure and larger surface roughness.

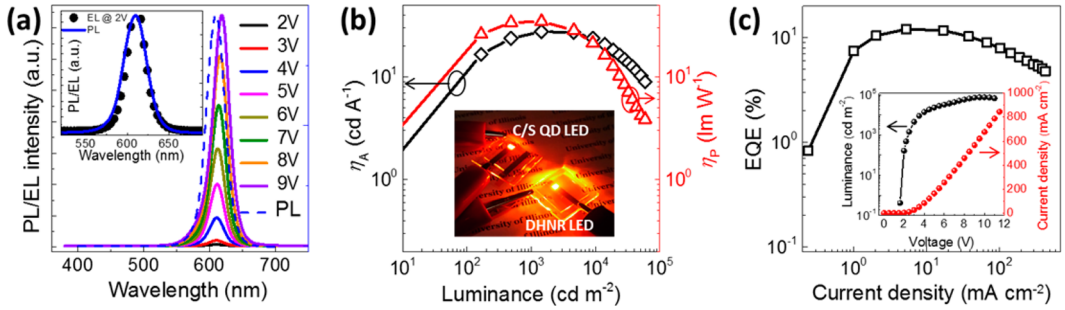

Figure 3. (a) EL spectra of a DHNR-LED at the indicated applied voltages along with normalized solution PL spectrum of the DHNRs. Inset shows a comparison of solution PL with low bias EL. (b) Dependence of current and power efficiencies on luminance and a photograph comparing the brightness of C/S QD-LED and DHNR-LED both operating at 4 V (inset). (c) External quantum efficiency (EQE) *vs* current density. Inset shows the dependence of luminance and current density on the applied voltage.

better match ETL, which should help to balance charge in DHNRs (see Supporting Information Figure S1). Furthermore, F_4TCNQ significantly alters HTL solubility enabling solution processing. As shown in Figure 2b and Supporting Information Figure S2, the thickness of pristine TFB film is reduced considerably while F_4TCNQ doped TFB films exhibit a very small thickness change upon chloroform (solvent for DHNRs) exposure. Aromatic amine-containing polymers can be cross-linked by TCNQ upon electron transfer[23] and we suspect that F_4TCNQ causes both hole doping and ionic cross-linking of TFB. This cross-linking can then explain the improved solvent resistance of HTL. Interestingly, surface roughness and contact angle remain essentially unchanged upon F_4TCNQ doping (Figures 2c-f), allowing for solution deposition of DHNRs without drastic changes to wetting behavior and DHNR orientation.

These advantages afforded by F_4TCNQ along with the benefits of the double heterojunction designed into DHNRs lead to an exceptional LED performance. Very narrow (full-width-at-half-maximum of 26 nm) and bright (76 000 cd m^{-2}) electroluminescence (EL) without parasitic emission from the transport layers is observed over the entire operation range with a threshold voltage (defined here as the voltage necessary to achieve 0.1 cd m^{-2}) of only ~1.55 V (Figure 3). The threshold voltage being significantly lower than that of the band gap of the emitter (~2 eV) is cur-

TABLE 1. Comparison of the PL and EL Characteristics of Current-State-of-the-Art of QD-LEDs with Those of DHNR-LEDs

Device structure	Emitting layer	λ_{max} (nm)	PL QY (%)	V_{on} (V)	Max. L (cd m^{-2})	Peak EQE (%)	Peak CE (cd A^{-1})	Peak PE (lm W^{-1})	Ref.
Conventional	CdSe/ZnS core/shell	600	~ 80	1.7	31,000	1.7	3.9	3.8	3
	CdSe/CdS/ZnS core/shell	618	> 70	<2.0	~16,500	~1.6	~3.5	4.25	5
	CdSe/CdZnS nanoplatelet	650	20 ~ 30	2~5	4 ,499	0.63	-	-	6
	CdS/CdSe/ZnSe DHNR	**612**	**~40**	**1.55**	**76,000**	**12.05**	**27.52**	**34.6**	**This work**
Inverted	CdSe/CdS core/shell	615	90	1.5	~50,000	18	19	25	1
	CdSe/CdS/ZnS core/shell	630	70~80	1.8	23,000	7.8	5.7	-	2
	CdSe/CdS/ZnS core/shell	630	70~80	1.8~2.0	57,350	-	5.78	7.12	9

rently under debate and may be associated with an Auger-related process[24] or the presence of a charge prior to biasing due to charge transfer from the adjacent transport layers.[25] While these characteristics are comparable to the best reported C/S QD-LEDs, current and power efficiencies of 27.5 cd A^{-1} and 34.6 lm W^{-1}, respectively, exceed all QD-LEDs of similar emission wavelength (Table 1). The maximum EQE of our DHNR-LEDs is found to be 12.05%. EQE *vs* voltage plots for various TFB/F_4TCNQ ratios examined here are shown in Supporting Information Figure S3.

A comparison of the average EQE, current and power efficiencies, and brightness (Figure 4) with respect to F_4TCNQ doping for DHNR- and C/S QD-LEDs (both fabricated in the same manner in the conventional structure) demonstrate that our DHNR design is also critical to the exceptional performance of DHNR-LEDs rather than improvements afforded by F_4TCNQ alone. Efficiencies of DHNR-LEDs are routinely 2 to 3 times higher and brighter EL can be readily seen by the naked eye (Figure 3b inset). Note that EQEs between 2 and 6% of our control C/S QD-LEDs with F_4TCNQ are among the highest reported values for red emitting QD-LEDs with conventional device structure.[3,26] High efficiencies of DHNR-LEDs are especially impressive and surprising in that the solution PL QY of DHNRs is only about half that of C/S QDs. A comparison of PL spectra of DHNRs and C/S QDs used here (normalized to absorbance at the excitation wavelength of 400 nm) along with PL spectrum of a reference dye are shown in Supporting Information Figure S4 to verify that the DHNRs have same PL QY as ref 19 and that the PL QY of C/S QDs is about twice as large.

QD-LEDs that require relatively high operating voltages may have low efficiencies due to high field induced charge separation reducing PL QYs.[27] High brightness at low voltages (*e.g.*, >10 000 cd m^{-2} already at 4 V bias) and therefore low operating field should contribute to high efficiencies but the staggered band offset between CdS and ZnSe should make charge separation easier. The rod geometry placing CdSe emitters relatively far away from each other and therefore minimizing energy transfer loss (similar to thick ZnS shell QD-LEDs[4] but without compromising turn-on voltage and power efficiency) is also likely to contribute to high efficiencies. A comparison of solution PL with low bias EL (Figure 3a inset) shows good overlap in peak position and line width supporting minimized energy transfer loss. However, these benefits alone cannot explain the 12% EQE which apparently *exceeds the expected upper limit*, suggesting that DHNRs provide yet additional benefits beyond improved carrier injection, low operating voltage and minimized energy transfer losses.

In general, EQE is given by

$$\mathrm{EQE} = (\gamma \times \eta_\gamma \times q_{\mathrm{PL}}) \times \eta_{\mathrm{out}} \quad (1)$$

The product in the parentheses is the IQE and η_{out} is the light outcoupling efficiency.[28] IQE is limited by the charge balance (γ), the radiative exciton production efficiency (η_γ), and the PL QY of the emitter (q_{PL}). Even if improvements due to F_4TCNQ and the additional reduction in HIB due to ZnSe of DHNRs allow us to reach ideal limits for γ and η_γ, q_{PL} = 40%[19] and the assumption of maximum η_{out} = 20%[29] limit the maximum EQE to 8%, well below our measured 12%. A histogram of EQEs with and without F_4TCNQ shown in Supporting Information Figure S5 demonstrates that 77% of the devices measured with optimum F_4TCNQ concentrations exhibit EQE > 8%. We believe that the rod shape and the directional type II band offset increase η_{out} limit.

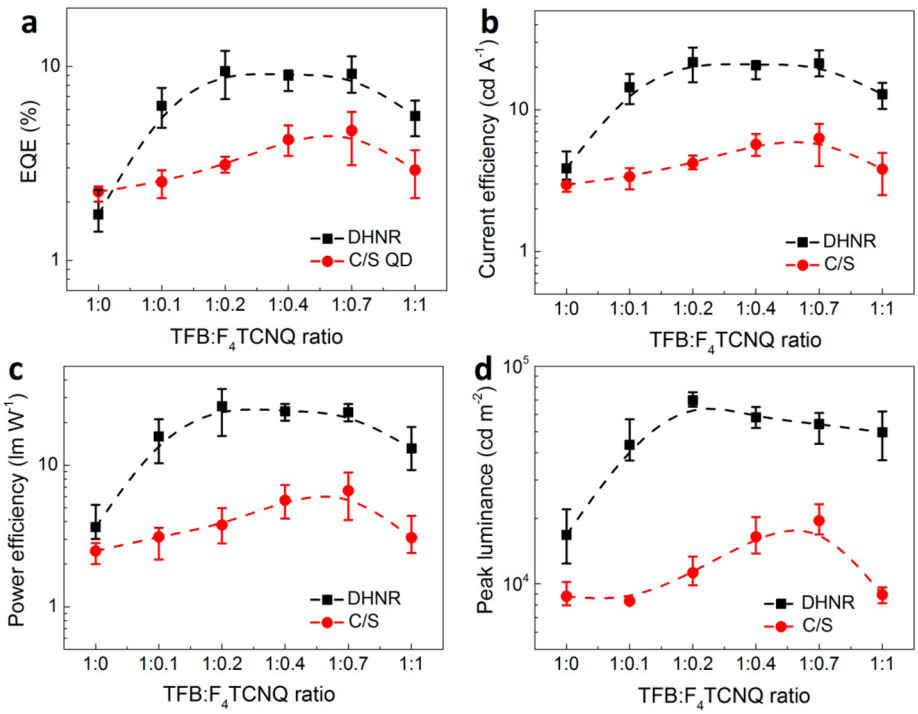

Figure 4. Comparison of the average (a) EQE, (b) current efficiency, (c) power efficiency, and (d) peak luminance as a function of F_4TCNQ doping ratio for DHNR-LEDs and C/S QD-LEDs. Each data point is averaged over 4−6 devices per data point with the error bars representing the maximum and the minimum values for a given F_4TCNQ doping condition. The drop in all values at 1:1 TFB/F_4TCNQ ratio for both C/S QD- and DHNR-LEDs likely arises from the solubility limit of F_4TCNQ.

In OLEDs, several known factors reduce light output including loss to surface plasmons and waveguide modes.[30] Such losses can be strongly dependent on the emitter dipole orientation.[31,32] For a simple OLED structure, random dipole orientation leads to $\eta_{out} \leq$ 20%, whereas surface parallel dipoles can theoretically lead to $\eta_{out} >$ 40%.[33−35] Given that the majority of DHNRs lie flat on the substrate (*e.g.*, SEM images of Figure 1e and Supporting Information Figure S6), we expect our DHNR-LEDs to fall close to the latter case. That is, the directionality of the type II staggered band offset (along the rod axis) between CdS and ZnSe that anisotropically surround the emitting CdSe center should induce a transition dipole along the rod axis. DHNRs lying mostly in-plane should then give rise to this transition dipole being oriented mainly parallel to the substrate. In-plane transition dipole orientation is well-known to reduce light outcoupling losses in OLEDs[33−36] and similar effects should be taking place for our DHNR-LEDs. Variable angle spectroscopic ellipsometry[31,36] indeed verify optical anisotropy in DHNR films. The complex refractive index of a DHNR film obtained from the uniaxial model is shown in Figure 5a. In particular, the ordinary (in-plane) extinction k_o is significantly larger than the extraordinary (out-plane) extinction k_e. C/S QD films do not exhibit significant optical anisotropy (Figure 5b). The measured k_o and k_e values correspond to an orientation order parameter $[(k_e - k_o)/(k_e + 2k_o)]$ of −0.47 for DHNRs and −0.07 for C/S QDs at 610 nm (near the emission wavelength) indicating that the transition dipole of DHNRs is nearly parallel to the substrate whereas that of C/S QDs are essentially randomly oriented. Therefore, we suggest that parallel orientation easily achieved for DHNRs and the resulting optical anisotropy significantly increase the upper limit of η_{out}, explaining the observed high EQE of 12%.

Finally, we note that there may be surrounding induced effects on the EL characteristics of C/S QDs and DHNRs that can complicate device performance analysis. For example, nearby metal surfaces and other factors can alter PL intensity and blinking,[37,38] making it difficult to compare radiative recombination in devices to solution PL. A more directly important effect here may be the possibility of CdSe QDs being charged even at zero-bias due to charge transfer from ZnO/Al layers and there is evidence that EQEs of CdSe-based C/S QD-LEDs depend on the negative trion PL rather than the neutral exciton PL QY.[25] While existing charges may help to explain the low, sub-band gap threshold voltages,[1,24] EQE dependence on the trion PL makes estimates with solution PL inappropriate, even as an upper limit, in analyzing EQE. However, the apparent reduction in PL of charged QDs is a topic of continuing debate,[25,39,40] and a recent study has shown that by suppressing nonradiative Auger recombination, trion PL can be as bright as exciton PL without the undesirable blinking behavior.[40] Rod shape[41] and directional type II band offset may help to suppress Auger recombination and therefore high EL from

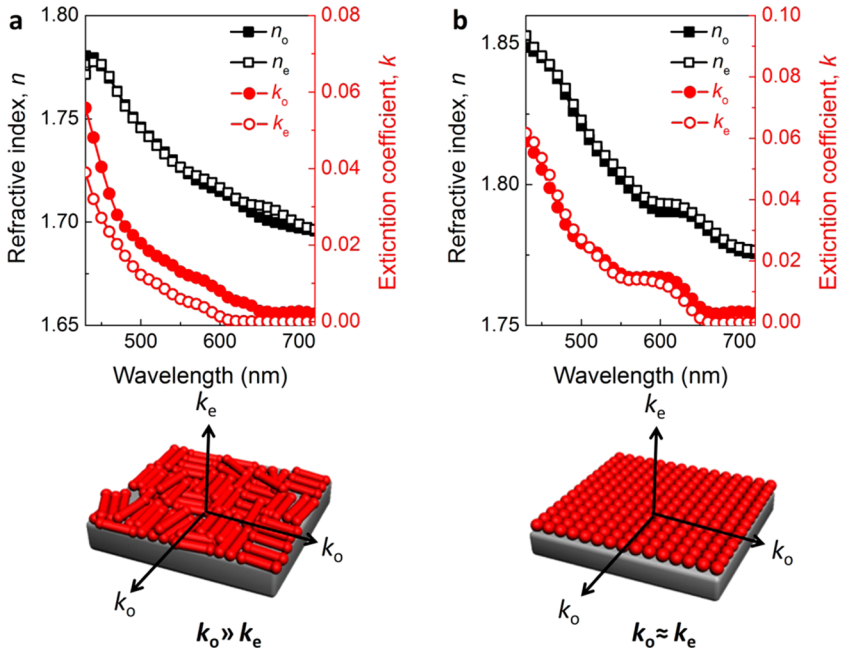

Figure 5. Ordinary (in-plane) real (n_o) and imaginary (k_o) parts of the refractive index and extraordinary (out-of-plane) components, n_e and k_e, measured by variable angle spectroscopic ellipsometry for (a) DHNR and (b) C/S QD films both spin-cast on Si wafer. SEM images of these two thin film samples used for ellipsometry along with their corresponding solution absorption spectra are shown in Supporting Information Figure S6.

charged DHNRs may be possible. However, it may be more likely that F_4TCNQ is counteracting the charging effects of ZnO ETL/Al cathode. During the preparation of this paper we became aware of two recent reports demonstrating that either using an insulating PMMA layer between ZnO ETL and the emitting layer[42] or controlling shell thickness[43] in C/S QD-LEDs to reduce charging of QDs can lead to record-breaking LED performances (*e.g.*, 20.5% EQE and >100 000 cd m^{-2}, respectively). These results are very impressive but the introduction of an insulating layer, whether in the form of a thin film or a shell on individual QDs, may lead to limitations especially in power efficiency. Our results using F_4TCNQ, if it also acted to counteract charging of C/S QDs and DHNRs, may be an alternative approach to this charging problem without compromising power efficiency (as suggested by the record efficiency of 34.6 lm W^{-1} for red QD-based LEDs demonstrated here). Further work along these lines should provide insights that facilitate new and exciting means of designing and utilizing double heterojunctions to manipulate optical processes in colloidal QDs.

CONCLUSION

In summary, we have demonstrated that anisotropic DHNRs in conjunction with an enhanced HTL can lead to remarkable LED performance in a conventional solution processed device structure. The benefits of introducing the hole dopant F_4TCNQ in the HTL are multifold including improved hole injection/transport and solvent resistance and, possibly, reduced zero-bias charging of the emitters without sacrificing power efficiency. The anisotropic shape and the band offsets designed into the DHNRs allow improved carrier injection, low operating voltage, minimized energy transfer losses, and enhanced light outcoupling. The DHNR-LEDs achieved here exhibit maximum brightness of 76 000 cd m^{-2}, current efficiency of 27.5 cd A^{-1}, and power efficiency of 34.6 lm W^{-1}. A very high EQE of 12% at PL QY of only 40% implies that there is a fundamentally different and higher efficiency limit to these DHNR-LEDs than other C/S QD-based LEDs. It is the optical anisotropy of the DHNRs that should increase the upper limit on light outcoupling, a new and, until now, unexplored aspect of these materials and their devices.

METHODS

Materials. Trioctylphosphine oxide (TOPO) (90%), trioctylphosphine (TOP) (90%), oleic acid (OA) (90%), trioctylamine (TOA) (90%), octadecene (ODE) (90%), 1-octanethiol (98.5%), CdO (99.5%), Zn acetate (99.99%), S powder (99.998%), and Se powder (99.99%) were obtained from Sigma-Aldrich. *N*-Octadecylphosphonic acid (ODPA) was obtained from PCI Synthesis. ACS grade chloroform and methanol were obtained from Fischer Scientific. All chemicals were used as received. Standard airless techniques were used in all syntheses.

Synthesis of DHNRs. CdS/CdSe/ZnSe DHNRs were synthesized following ref 19. Briefly, CdO powder (0.128 g) and ODPA (0.668 g) in TOPO (2.0 g) were degassed at 150 °C for 30 min, then heated to 350 °C for 2 h. TOP:S (2.0 mL of 0.25 M solution) was quickly injected at 370 °C and stirred for 20 min at 330 °C. TOP:Se (1.0 mL of 0.25 M solution) was then slowly injected

(4 mL h^{-1}). After 10 min, the reaction mixture was cooled to room temperature and the resulting CdS/CdSe nanorods were precipitated and redissolved in ~4 mL of chloroform. A mixture of Zn acetate (0.184 g) and OA (1.13 mL) in ODE (6 mL) was degassed and heated to 250 °C. After 1 h, Zn containing reaction mixture was cooled to 60 °C and CdS/CdSe nanorod solution (2 mL) was injected. After heating to 250 °C, TOP:Se (1.0 mL of 0.25 M solution) was slowly injected (4 mL h^{-1}). The reaction mixture was then heated to 300 °C for 5 min before cooling to room temperature.

Synthesis of C/S QDs. CdSe/CdS/ZnS C/S QDs were prepared similar to ref 44. After CdO powder (0.206 g) and OA (2.0 mL) were degassed in TOA (40 mL) at 150 °C for 30 min and the mixture heated to 300 °C, TOP:Se (0.4 mL of 1.0 M solution) was swiftly injected into the reaction mixture. After 45 s, 1-octanethiol (0.21 mL) in TOA (6 mL) was slowly injected (1 mL min^{-1}). The reaction mixture was then allowed to stir for 30 min at 300 °C. Sixteen milliliters of Zn-oleate solution, prepared in a separate flask by stirring Zn acetate (0.92 g) and OA (3.2 mL) in TOA (20 mL) at 250 °C for 60 min, followed by 1.12 mL of 1-octanethiol in 6 mL of TOA, was injected at 1 mL min^{-1}. After 30 min, the solution was cooled to room temperature.

Device Fabrication. LEDs were fabricated on prepatterned and precleaned ITO on glass substrates (sheet resistance of 15−25 Ω $\square^{-1}$). PEDOT:PSS (Clevios P VP AI 4083) was spin-coated onto ITO (4000 rpm) and baked at 120 °C in air (5 min) and 180 °C in a glovebox (15 min). Then, 10 mg mL^{-1} solution of TFB (H.W. Sands Corp.) in *m*-xylene or appropriate amount of F_4TCNQ (Sigma-Aldrich) dissolved in 5 mg mL^{-1} solution of TFB in *m*-xylene to achieve desired weight ratios was spin-coated (3000 rpm) and baked at 180 °C in a glovebox (30 min). DHNRs (60 mg mL^{-1}) or C/S QDs (30 mg mL^{-1}) in chloroform after washing twice with 1:1 volume ratio of chloroform and methanol was spin-cast (2000 rpm), then subsequently annealed at 180 °C in a glovebox (30 min). ZnO (~30 mg mL^{-1} in butanol, prepared following ref 19) was then spin-coated (3000 rpm) and annealed at 100 °C (30 min). A 100 nm thick Al cathode was then deposited by electron-beam evaporation. LEDs were encapsulated with a cover glass using epoxy (NOA 86) in a glovebox.

Characterization. TEM and SEM images were obtained on JEOL 2100 Cryo TEM and Hitachi S4800 SEM, respectively. UPS was performed using He I photon line ($h\nu$ = 21.2 eV) at ~10^{-9} Torr (PHI 5400). Tapping-mode AFM and contact angle measurements were carried out on an Asylum Research MFP-3D AFM and a Rame-Hart model 500 goniometer/tensiometer, respectively. LED characteristics were recorded using a Spectrascan PR-655 spectroradiometer coupled with a Keithely 2602B source-measure unit. EQE was calculated as the ratio of the number of photons emitted to the number of electrons injected. Current and power efficiencies were obtained as the ratio of the output luminance to the driving current density and the ratio of the luminous flux output to the driving electrical power, respectively. All device measurements were performed in air. UV−vis absorption spectra were obtained with an Agilent 8453 spectrometer. PL spectra were collected with Horiba Jobin Yvon FluoroMax-3. Ellipsometry of DHNR and C/S QD films on Si substrates were collected in the wavelength range of 400−900 nm at incidence angles of 50, 60, and 70° on a J. A. Woollam VASE Ellipsometer. Data analysis was performed using WVASE32 software. The thicknesses of the films were first determined using Cauchy model, then Kramers−Kronig consistent model was used to calculate the optical constants. Anisotropic optical constants of the films were obtained using the uniaxial anisotropic model by minimizing the mean square error.

Conflict of Interest: The authors declare no competing financial interest.

Acknowledgment. The authors thank Peter Trefonas and Jong Keun Park for helpful discussions and for suggesting solvent strip tests and Kenneth Kearns for helpful insights on ellipsometry measurements. This material is based upon work supported by the Dow Chemical Company and U.S. NSF (Grant No. 1153081). Experiments were carried out in part in the Frederick Seitz Materials Research Laboratory Central Facilities, University of Illinois.

Supporting Information Available: Additional UPS, electrical, absorption, PL, and EQE data. This material is available free of charge *via* the Internet at http://pubs.acs.org.

REFERENCES AND NOTES

1. Mashford, B. S.; Stevenson, M.; Popovic, Z.; Hamilton, C.; Zhou, Z.; Breen, C.; Steckel, J.; Bulovic, V.; Bawendi, M.; Coe-sullivan, S.; *et al.* High-efficiency Quantum-dot Light-emitting Devices with Enhanced Charge Injection. *Nat. Photonics* **2013**, *7*, 407–412.
2. Kwak, J.; Bae, W. K.; Lee, D.; Park, I.; Lim, J.; Park, M.; Cho, H.; Woo, H.; Yoon, D. Y.; Char, K.; *et al.* Bright and Efficient Full-Color Colloidal Quantum Dot Light-Emitting Diodes Using an Inverted Device Structure. *Nano Lett.* **2012**, *12*, 2362–2366.
3. Qian, L.; Zheng, Y.; Xue, J.; Holloway, P. H. Stable and Efficient Quantum-Dot Light-Emitting Diodes Based on Solution-Processed Multilayer Structures. *Nat. Photonics* **2011**, *5*, 543–548.
4. Lee, K.-H.; Lee, J.-H.; Kang, H.-D.; Park, B.; Kwon, Y.; Ko, H.; Lee, C.; Lee, J.; Yang, H. Over 40 cd/A Efficient Green Quantum Dot Electroluminescent Device Comprising Uniquely Large-Sized Quantum Dots. *ACS Nano* **2014**, *8*, 4893–4901.
5. Kim, T.; Cho, K.; Lee, E. K.; Lee, S. J.; Chae, J.; Kim, J. W.; Kim, D. H.; Kwon, J.; Amaratunga, G.; Lee, S. Y.; *et al.* Full-Colour Quantum Dot Displays Fabricated by Transfer Printing. *Nat. Photonics* **2011**, *5*, 176–182.
6. Chen, Z.; Nadal, B.; Mahler, B.; Aubin, H.; Dubertret, B. Quasi-2D Colloidal Semiconductor Nanoplatelets for Narrow Electroluminescence. *Adv. Funct. Mater.* **2014**, *24*, 295–302.
7. Sun, Q.; Subramanyam, G.; Dai, L.; Check, M.; Campbell, A.; Naik, R.; Grote, J.; Wang, Y. Highly Efficient Quantum-Dot Light-Emitting Diodes with DNA-CTMA as a Combined Hole-Transporting and Electron-Blocking Layer. *ACS Nano* **2009**, *3*, 737–743.
8. Zhao, J.; Bardecker, J. a; Munro, A. M.; Liu, M. S.; Niu, Y.; Ding, I.-K.; Luo, J.; Chen, B.; Jen, A. K.-Y.; Ginger, D. S. Efficient CdSe/CdS Quantum Dot Light-Emitting Diodes Using a Thermally Polymerized Hole Transport Layer. *Nano Lett.* **2006**, *6*, 463–467.
9. Kim, H.-M.; bin Mohd Yusoff, A. R.; Youn, J.-H.; Jang, J. Inverted Quantum-Dot Light Emitting Diodes with Cesium Carbonate Doped Aluminium-Zinc-Oxide as the Cathode Buffer Layer for High Brightness. *J. Mater. Chem. C* **2013**, *1*, 3924–3930.
10. Milliron, D. J.; Hughes, S. M.; Cui, Y.; Manna, L.; Li, J.; Wang, L.-W.; Alivisatos, A. P. Colloidal Nanocrystal Heterostructures with Linear and Branched Topology. *Nature* **2004**, *430*, 190–195.
11. Shieh, F.; Saunders, A. E.; Korgel, B. A. General Shape Control of Colloidal CdS, CdSe, CdTe Quantum Rods and Quantum Rod Heterostructures. *J. Phys. Chem. B* **2005**, *109*, 8538–8542.
12. Halpert, J. E.; Porter, V. J.; Zimmer, J. P.; Bawendi, M. G. Synthesis of CdSe/CdTe Nanobarbells. *J. Am. Chem. Soc.* **2006**, *128*, 12590–12591.
13. Kumar, S.; Jones, M.; Lo, S. S.; Scholes, G. D. Nanorod Heterostructures Showing Photoinduced Charge Separation. *Small* **2007**, *3*, 1633–1639.
14. McDaniel, H.; Zuo, J. M.; Shim, M. Anisotropic Strain Induced Curvature in Type II CdSe/CdTe Nanorod Heterostructures. *J. Am. Chem. Soc.* **2010**, *132*, 3286–3288.
15. Talapin, D. V.; Koeppe, R.; Gotzinger, S.; Kornowski, A.; Lupton, J. M.; Rogach, A. L.; Benson, O.; Feldmann, J.; Weller, H. Highly Emissive Colloidal CdSe/CdS Heterostructures of Mixed Dimensionality. *Nano Lett.* **2003**, *3*, 1677–1681.
16. Deutsch, Z.; Neeman, L.; Oron, D. Luminescence Upconversion in Colloidal Double Quantum Dots. *Nat. Nanotechnol.* **2013**, *8*, 649–653.

17. Hikmet, R. A. M.; Chin, P. T. K.; Talapin, D. V.; Weller, H. Polarized-Light-Emitting Quantum-Rod Diodes. *Adv. Mater.* **2005**, *17* (11), 1436–1439.
18. Rizzo, A.; Nobile, C.; Mazzeo, M.; De Giorgi, M.; Fiore, A.; Carbone, L.; Cingolani, R.; Manna, L.; Gigli, G. Polarized Light Emitting Diode by Long-Range Nanorod Self-Assembling on a Water Surface. *ACS Nano* **2009**, *3*, 1506–1512.
19. Oh, N.; Nam, S.; Zhai, Y.; Deshpande, K.; Trefonas, P.; Shim, M. Double-Heterojunction Nanorods. *Nat. Commun.* **2014**, *5*, 3642.
20. Chen, Y.; Xia, Y.; Smith, G. M.; Sun, H.; Yang, D.; Ma, D.; Li, Y.; Huang, W.; Carroll, D. L. Solution-Processable Hole-Generation Layer and Electron-Transporting Layer: Towards High-Performance, Alternating-Current-Driven, Field-Induced Polymer Electroluminescent Devices. *Adv. Funct. Mater.* **2014**, *24*, 2677–2688.
21. Lim, E.; Jung, B.-J.; Chikamatsu, M.; Azumi, R.; Yoshida, Y.; Yase, K.; Do, L.-M.; Shim, H.-K. Doping Effect of Solution-Processed Thin-Film Transistors Based on Polyfluorene. *J. Mater. Chem.* **2007**, *17*, 1416–1420.
22. Abdula, D.; Shim, M. Performance and Photovoltaic Response of Polymer Doped Carbon Nanotube p-n Diodes. *ACS Nano* **2008**, *2*, 2154–2159.
23. Yamaguchi, I.; Mizoguchi, N. Π-Conjugated Polyphenylene Gels with Charge Transfer Structures Assisted by TCNQ. *React. Funct. Polym.* **2011**, *71*, 1166–1171.
24. Qian, L.; Zheng, Y.; Choudhury, K. R.; Bera, D.; So, F.; Xue, J.; Holloway, P. H. Electroluminescence from Light-Emitting Polymer/ZnO Nanoparticle Heterojunctions at Sub-Bandgap Voltages. *Nano Today* **2010**, *5*, 384–389.
25. Bae, W. K.; Park, Y.-S.; Lim, J.; Lee, D.; Padilha, L. A.; McDaniel, H.; Robel, I.; Lee, C.; Pietryga, J. M.; Klimov, V. I. Controlling the Influence of Auger Recombination on the Performance of Quantum-Dot Light-Emitting Diodes. *Nat. Commun.* **2013**, *4*, 2661.
26. Zheng, Y.; Qian, L.; Yang, Y.; Titov, A.; Hyvonen, J.; Cao, W.; Xue, J.; Holloway, P. H. High Efficiency and Long Lifetime Quantum Dot-Light Emitting Diodes for Flat Panel Display Applications. *SID Int. Sypm. Dig. Tech. Pap.* **2013**, *44*, 221–223.
27. Bozyigit, D.; Yarema, O.; Wood, V. Origins of Low Quantum Efficiencies in Quantum Dot LEDs. *Adv. Funct. Mater.* **2013**, *23*, 3024–3029.
28. Nakanotani, H.; Higuchi, T.; Furukawa, T.; Masui, K.; Morimoto, K.; Numata, M.; Tanaka, H.; Sagara, Y.; Yasuda, T.; Adachi, C. High-Efficiency Organic Light-Emitting Diodes with Fluorescent Emitters. *Nat. Commun.* **2014**, *5*, 4016.
29. Meerheim, R.; Lussem, B.; Leo, K. Efficiency and Stability of P-I-N Type Organic Light Emitting Diodes for Display and Lighting Applications. *Proc. IEEE* **2009**, *97*, 1606–1626.
30. Meerheim, R.; Furno, M.; Hofmann, S.; Lüssem, B.; Leo, K. Quantification of Energy Loss Mechanisms in Organic Light-Emitting Diodes. *Appl. Phys. Lett.* **2010**, *97*, 253305.
31. Lin, H.-W. Anisotropic Optical Properties and Molecular Orientation in Vacuum-Deposited ter(9,9-Diarylfluorene)s Thin Films Using Spectroscopic Ellipsometry. *J. Appl. Phys.* **2004**, *95*, 881–883.
32. Flämmich, M.; Gather, M. C.; Danz, N.; Michaelis, D.; Bräuer, A. H.; Meerholz, K.; Tünnermann, A. Orientation of Emissive Dipoles in OLEDs: Quantitative *in Situ* Analysis. *Org. Electron.* **2010**, *11*, 1039–1046.
33. Kim, S.-Y.; Jeong, W.-I.; Mayr, C.; Park, Y.-S.; Kim, K.-H.; Lee, J.-H.; Moon, C.-K.; Brütting, W.; Kim, J.-J. Organic Light-Emitting Diodes with 30% External Quantum Efficiency Based on a Horizontally Oriented Emitter. *Adv. Funct. Mater.* **2013**, *23*, 3896–3900.
34. Kim, J.-S.; Ho, P. K. H.; Greenham, N. C.; Friend, R. H. Electroluminescence Emission Pattern of Organic Light-emitting Diodes: Implications for Device Efficiency Calculations. *J. Appl. Phys.* **2000**, *88*, 1073–1081.
35. Brütting, W.; Frischeisen, J.; Schmidt, T. D.; Scholz, B. J.; Mayr, C. Device Efficiency of Organic Light-emitting Diodes: Progress by Improved Light Outcoupling. *Phys. Status. Solidi A* **2013**, *210*, 44–65.
36. Yokoyama, D.; Sakaguchi, A.; Suzuki, M.; Adachi, C. Horizontal Molecular Orientation in Vacuum-Deposited Organic Amorphous Films of Hole and Electron Transport Materials. *Appl. Phys. Lett.* **2008**, *93*, 173302.
37. Krauss, T. D.; Peterson, J. J. Bright Future for Fluorescence Blinking in Semiconductor Nanocrystals. *J. Phys. Chem. Lett.* **2010**, *1*, 1377–1382.
38. Ito, Y.; Matsuda, K.; Kanemitsu, Y. Mechanism of Photoluminescence Enhancement in Single Semiconductor Nanocrystals on Metal Surfaces. *Phys. Rev. B* **2007**, *75*, 033309.
39. Galland, C.; Ghosh, Y.; Steinbrück, A.; Sykora, M.; Hollingsworth, J. A.; Klimov, V. I.; Htoon, H. Two Types of Luminescence Blinking Revealed by Spectroelectrochemistry of Single Quantum Dots. *Nature* **2011**, *479*, 203–207.
40. Qin, W.; Liu, H.; Guyot-Sionnest, P. Small Bright Charged Colloidal Quantum Dots. *ACS Nano* **2014**, *8*, 283–291.
41. Padilha, L. A.; Stewart, J. T.; Sandberg, R. L.; Bae, W. K.; Koh, W.-K.; Pietryga, J. M.; Klimov, V. I. Aspect Ratio Dependence of Auger Recombination and Carrier Multiplication in PbSe Nanorods. *Nano Lett.* **2013**, *13*, 1092–1099.
42. Dai, X.; Zhang, Z.; Jin, Y.; Niu, Y.; Cao, H.; Liang, X.; Chen, L.; Wang, J.; Peng, X. Solution-processed, High-Performance Light-Emitting Diodes Based on Quantum Dots. *Nature* **2014**, *515*, 96–99.
43. Lim, J.; Jeong, B. G.; Park, M.; Kim, J. K.; Pietryga, J. M.; Park, Y.-S.; Klimov, V. I.; Lee, C.; Lee, D. C.; Bae, W. K. Influence of Shell Thickness on the Performance of Light-Emitting Devices Based on CdSe/$Zn_{1-x}Cd_xS$ Core/Shell Heterostructured Quantum Dots. *Adv. Mater.* **2014**, *26*, 8034–8040.
44. Lim, J.; Jun, S.; Jang, E.; Baik, H.; Kim, H.; Cho, J. Preparation of Highly Luminescent Nanocrystals and Their Application to Light-Emitting Diodes. *Adv. Mater.* **2007**, *19*, 1927–1932.